Energy harvesting analysis in railway bridges: an approach based on modal decomposition

A. Romero[a,*], J.C. Cámara-Molina[a], E. Moliner[b], P. Galvín[a,c], M.D. Martínez-Rodrigo[b]

[a] *Escuela Técnica Superior de Ingeniería, Universidad de Sevilla, Camino de los Descubrimientos s/n, ES-41092 Sevilla, Spain*

[b] *Universitat Jaume I, Department of Mechanical Engineering and Construction, Avda. Sos Baynat s/n, ES-12071 Castellón, Spain*

[c] *Laboratory of Engineering for Energy and Environmental Sustainability, Universidad de Sevilla, Camino de los Descubrimientos s/n, ES-41092 Sevilla, Spain*

Abstract

In this paper the authors investigate the energy harvesting in railway bridges and analyse the performance under different operational conditions. An approximation based on modal superposition is proposed for the computation of the energy harvested from train-induced bridge vibration. This approach is consistent with the analytical modal solutions of the simply-supported Bernouilli-Euler beam transverse response under moving loads. The influence of the bridge maximum dynamic response and cancellation phenomena, the tuning effect of the harvester device and the relevance of different modal contributions on the harvested energy are studied using a single-degree of freedom system as a simplistic mechanical approach. Later, a piezoelectrically coupled lumped parameter model is used to investigate the available energy due to High-Speed train passages at different circulating speeds. Finally, the feasibility of energy harvesting is evaluated from the experimental data measured by the authors in a railway bridge from the Madrid-Sevilla High-Speed line. The obtained results allow quantifying the harvested energy in a time window of three and a half hours and twenty train passages.

Keywords: Energy harvesting, railway bridges, High-Speed train, cantilever bimorph beam, piezoelectric device

1. Introduction

The construction of the trans-European network, including the railway network, is of utmost importance for a balanced and sustainable development of the European Union (EU). The European Commission [1] has adopted a strategy to promote the development of an effective EU rail infrastructure, establishing an attractive and truly open rail market in order to increase by 30 to 50 per cent the passenger transport by

*Corresponding author.
Email address: aro@us.es (A. Romero)

2050 [2]. The increase of railway traffic will require adequate maintenance of the infrastructure to ensure the required levels of quality, safety, and reliability. Moreover, this increment and the ageing of the railway lines will lead to the need of further development of monitoring systems and maintenance procedures to prevent damages associated to the dynamic effects on the infrastructure.

In particular, the dynamic effects in railway bridges have become an issue of interest and concern for scientists and engineers in the last decades, especially since the advent of High-Speed lines (HSL) [3–6]. An excessive level of vertical accelerations at the deck platform (greater than 3.5 or $5\,\mathrm{m/s^2}$ in ballast or slab track bridges, respectively), can lead to misalignment of the rails as a result of premature deconsolidation of the ballast layer, to the loose of contact between wheel and rail, with the subsequent increase of the risk of derailment, to structural fatigue problems in the long term or to an increase of the maintenance costs in the best scenario. Specifically, the Spanish railway network currently has a total of 135 km of track that runs over more than 6000 bridges. The infrastructure maintenance includes the auscultation of 250 bridges and conducting 25 to 30 load tests every year. This situation may also apply to other EU countries.

Nowadays, the number of R&D&i projects addressing the development of new management systems permitting preventive and efficient maintenance of the infrastructure grows every year. Many of them aim a real-time monitoring of the conservation state. These management models extensively make use of microelectromechanical systems (MEMS) that include accelerometers, gyroscopes, inclinometers, pressure sensors, among others. Increasingly, remote and distributed detection systems are used to perform this task [7–9]. One of the most limiting factors for sensor networks used in railway monitoring applications is the lack of a long-term and low maintenance power supply. Most existing systems require battery changes, and the impossibility of access and infrequent maintenance operations can limit their practical implementation.

Energy harvesting is becoming an alternative to provide energy supply for nodes and sensors of monitoring systems in remote areas [10, 11]. The piezoelectric energy harvesting systems are a widespread and popular energy source to overcome the high degree of uncertainty in some applications caused by weather conditions as occurs in photovoltaic power systems. Many investigations have proposed mechanical devices to produce the necessary electrical energy from its own response to be used in small power devices and sensors based on the piezoelectric (PZT) effect. Common realizations of piezoelectric energy harvesters are the bimorph cantilever or end–end clamped beams, consisting of rectangular plates with two PZT layers. These systems have a power generation capability from micro to milliwatts from ambient vibrations in a frequency range of $5 - 100\,\mathrm{Hz}$ as referenced in [12]. Peigney and Siegert [13] studied energy harvesting from traffic-induced vibrations in bridges. A piezoelectric harvester was developed and tested, and the mean power due to traffic load was 0.03 mW for a voltage between 1.8 and 3.6 V. The authors concluded that the harvested energy could be used to feed health monitoring sensor nodes. Also, Song [29] studied the application of energy harvesting systems in railway bridges and found the root-mean-squared value of the output voltage varying in the range $0.7 - 6\,\mathrm{V}$ in single-span bridges. Takeya et al. [30] proposed a two-degree of freedom energy

harvester that enhanced the single-mass system for power generation.

In this context, the research presented herein deals with the application of energy harvesting from railway induced vibrations at the bridge structure. Previous works [14–16] have aimed to evaluate the feasibility of using piezoelectric devices for energy harvesting from track vibration. Nelson et al. [17] developed an inductive voice coil harvesting device directly excited by the rail vertical displacement. The power found in a field test was near to 1 mW for a train passage at 20 km/h. Tianchen et al. [18] tested a drum transducer installed under the sleeper for energy harvesting in railway tracks. The power obtained in a laboratory test was 0.1 mW (2.31 mJ) for a moving load travelling at 0.5 km/h. An important drawback of energy harvesting systems is related to the fact that the devices performance is limited to very narrow frequency bands around the resonance frequency, as mentioned by Erturk and Inman [19]. The output power drastically reduces if the excitation frequency slightly deviates from the resonance condition when the generator is not adequately tuned. More specifically, Ali et al. [20] investigated the feasibility of energy harvesting in highway bridges, taking into account that structural vibrations due to a vehicle passage can be considered as a source of energy. The analysis was based on the bridge modal decomposition in the frequency domain using the solution of a simply supported beam. The natural frequency of the harvester was tuned to the fundamental frequency of the bridge. Gatti et al. [21] studied the possibility of energy harvesting from track vibration during train passage using a mechanical single degree of freedom model. The authors found that the optimum energy harvested was proportional to the square of the amplitude and duration of the acceleration. They found an energy level related to the mass device of 0.25 J/kg tuned to 17 Hz from sleeper vibration. Milne et al. [22] studied the properties of the train load frequency that optimised the collected energy. The identified peaks mainly depend on the geometry of the train type, axle and bogie distances. Similarly, Cleante et al. [23] analysed the frequency content of experimental track vibration data, concluding that the train wheelset acts as a bandpass filter and limits the sleeper response at low frequencies for energy harvesting. Cahill et al. [24] investigated the possibility of energy harvesting from train-induced vibration in bridges and its application in structural health monitoring. The power found in train passages was below one milliwatt.

Later, Cahill et al. [25] investigated the feasibility of damage detection directly from harvested energy, considering that power varies from the undamaged to the damaged state of the bridge. The authors studied the sensitivity of the harvester to the road surface, bridge-vehicle interaction, and damage level. The analysis concluded that variations in the long-term of the harvested energy can be indicative of changes in the bridge flexural stiffness. Also, Cahill et al. [26] presented an experimental procedure to verify a piezoelectric energy harvester for railway bridges under operational conditions based on theoretical benchmarking, fabrication, calibration, and experimental validation. The voltage was found below one volt during the test for a harvester connected to a resistive load of 1 MΩ. Moreover, Cahill et al. [27] developed an energy harvester device for monitoring a full-scale railway bridge under operational conditions from voltage output data. The train passage was identified from data of harvested energy. Similarly, Fitzgerald et al. [28] proposed a damage

detection procedure using only a cantilever energy harvester device rather than an accelerometer to avoid the power consumption in the measurement. Then, the energy requirement is related to the storage and transmission of voltage data. The proposed procedure was tested in a laboratory-scale bridge to detect frequency changes due to structural damage. Although the power requirement can be ideally fulfilled by the harvester, the authors pointed out the need to investigate the energy available in the vibration of the bridge.

The novelty of this work includes the study of energy harvesters performance on railway bridges under different train circulating conditions. An approach based on modal superposition in the frequency domain is proposed for the estimation of the energy harvested from train-induced bridge vibration. This approach is consistent with the modal decomposition used in Reference [20] for the solution of bridge response under moving loads but, moreover, it founds that energy harvesting due to train passage can be obtained as the superposition of energy modal contributions. This approach is advantageous since the railway bridge response is generally governed by the contribution of only a few modes of vibration. Some of the issues in the previously referred works are investigated. The influence of the train speed and the bridge and harvester dynamic properties are analysed in-depth in the following sections to assess the energy harvested from train-induced vibration. The formulation and the approach adopted for the analysis are presented in Section 2. The governing equations of a coupled lumped parameter model for a cantilever bimorph beam are briefly described. Later, the proposed approach is used in Section 3 to study energy harvesting in simply-supported bridges. Maximum free vibration, cancellation phenomena, and energy harvesting under a single moving load are analysed. This analysis is complementary to the results presented by Ali et al. [20] for the response of highway bridges due to a single moving load. In this work, the results can be related to the amplification of the structure at resonance when traversed by a set of equidistant loads. Finally, a case study is presented and investigated in Section 4 using experimental data of an existing railway bridge. The main results and conclusions drawn from this research are summarised in Section 5.

2. Formulation and approach adopted for the analysis

The proposed approach considers an energy harvesting device attached to the bridge at a section defined by the x coordinate (see Figure 1). This device is subjected to the vertical vibration of the bridge $z_b(x,t)$ induced by a moving load p travelling at constant speed V. Following, the equilibrium equations of both systems, bridge and harvester, are formulated, and an approach based on modal superposition is proposed to assess the available energy in different conditions. Two strategies are presented to represent the device behaviour: *i*) an uncoupled mechanical model to evaluate the energy associated to the bridge vibration, and *ii*) a piezoelectric-mechanical coupled model to compute the electrical energy. In both cases, an equivalent lumped model is used to represent the bimorph device.

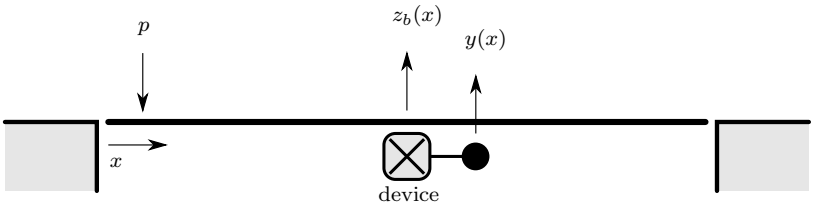

Figure 1: Scheme of bridge/harvester system.

2.1. The mechanical lumped parameter model

Typically, a lumped mass model is used to represent the dynamic behaviour of a cantilever beam with a tip mass for piezoelectric energy harvesting (Figure 1). The natural frequency ω of a uniform cantilever beam in transverse vibrations can be approximated from an equivalent mass m (sum of the beam effective mass and the mass of the tip) and the beam stiffness k computed from the distributed parameter model [31]. Then, the equilibrium equation of the harvester device represented as a single degree of freedom with base excitation is:

$$\ddot{y}(t) + 2\zeta\omega\dot{y}(t) + \omega^2 y(t) = -\ddot{z}_b(x,t) \tag{1}$$

where $y(t)$ denotes the vertical displacement of the lumped mass, ζ the damping factor, and $\ddot{z}_b(x,t)$ the support excitation which coincides with the bridge acceleration at coordinate x where the harvester is attached. In what follows an upper dot denotes time derivative.

In this section, a linear viscous damping coefficient $c = 2\zeta\sqrt{km}$ is considered to model both mechanical and electrical energy dissipation of the device. The damping coefficient is used to represent the energy transfer from the base vibration into the harvester system [32]. Then, the instantaneous power corresponds to the power absorbed by the harvester plus the kinetic energy. The mechanical energy in the system at period T is a function of the vibration velocity:

$$E = c\int_0^T |\dot{y}(t)|^2\, dt \tag{2}$$

The energy absorbed or dissipated by the damper (second term of the first member of Equation 1) is considered harvested energy. This approach is valid only for harvesters in which the electrical damping term is proportional to the velocity as occurs in electromagnetic converters [33, 34]. However, the approach adopted in this section facilitates understanding the energy transfer from the structure to the harvester as it is referred in [32, 34].

The previous equation can be expressed in terms of the Fourier transform of the harvester velocity according to the Parseval's theorem as:

$$E = c \int_{-\infty}^{\infty} |\dot{y}(\overline{\omega})|^2 \, d\overline{\omega} \tag{3}$$

where the system is assumed to be idle outside the time interval T to fulfil this identity. Also, Equation 3 can be rewritten in terms of the displacement as:

$$E = c \int_{-\infty}^{\infty} |\iota\overline{\omega} y(\overline{\omega})|^2 \, d\overline{\omega} \tag{4}$$

where the unit imaginary number is denoted by the Greek letter ι to prevent confusion with subscript i used in posterior derivations.

The displacement of the harvesting device is given by the vertical displacement of the bridge at location x:

$$y(\overline{\omega}) = m\overline{\omega}^2 H(\overline{\omega}) z_b(x, \overline{\omega}) \tag{5}$$

where $H(\overline{\omega})$ is the frequency response function of the device, that depends on the frequency ratio $\beta = \overline{\omega}/\omega$:

$$H(\overline{\omega}) = \frac{1}{k}\left[\frac{1}{(1-\beta^2) + 2\iota\zeta\beta}\right] \tag{6}$$

Then, the system response is properly defined when the bridge displacement $z_b(x, \overline{\omega})$ is known. In what follows, modal coordinates Z_{bj} are used to represent the bridge modal amplitudes in order to express the bridge vertical displacement as the superposition of the first N modes of vibration $\phi_{bj}(x)$:

$$z_b(x, \overline{\omega}) = \sum_{j=1}^{N} \phi_{bj}(x) Z_{bj}(\overline{\omega}) \tag{7}$$

Thus, the harvester displacement is obtained by substituting Equation 7 into Equation 5 in terms of the bridge transfer function H_{bj} and the moving load spectrum p_{bj} for the jth mode:

$$\begin{aligned} y(\overline{\omega}) &= m\overline{\omega}^2 H(\overline{\omega}) \sum_{j=1}^{N} \phi_{bj}(x) Z_{bj}(\overline{\omega}) \\ &= m\overline{\omega}^2 H(\overline{\omega}) \sum_{j=1}^{N} \phi_{bj}(x) H_{bj}(\overline{\omega}) p_{bj}(\overline{\omega}) \end{aligned} \tag{8}$$

Therefore, the energy in the system is obtained by substituting the previous definition into Equation 4:

$$\begin{aligned} E &= c\int_{-\infty}^{\infty}\left|\iota\overline{\omega}^3 mH(\overline{\omega})\sum_{j=1}^{N}\phi_j(x)H_{bj}(\overline{\omega})p_{bj}(\overline{\omega})\right|^2 d\overline{\omega} \\ &= c\int_{-\infty}^{\infty}\left|\sum_{j=1}^{N}C_j(\overline{\omega})\right|^2 d\overline{\omega} \end{aligned} \tag{9}$$

where C_j denotes the contribution of the jth mode shape to the total energy. This expression can be rewritten for a discrete-time signal of length M that would be helpful for experimental studies as follows:

$$E = \frac{c}{M}\sum_{i=1}^{M}\left|\sum_{j=1}^{N}C_j(\overline{\omega}_i)\right|^2 \tag{10}$$

Following, the total energy is approximated as the superposition of modal contributions C_j. Equation 10 can be expanded as:

$$\begin{aligned} E &= \frac{c}{M}\sum_{i=1}^{M}\left[\left(\sum_{j=1}^{N}C_j(\overline{\omega}_i)\right)\left(\sum_{j=1}^{N}C_j^*(\overline{\omega}_i)\right)\right] \\ &= \frac{c}{M}\sum_{i=1}^{M}\left[\sum_{j=1}^{N}|C_j(\overline{\omega}_i)|^2 + 2\sum_{k>j}^{N}\Re(C_j(\overline{\omega}_i)C_k(\overline{\omega}_i))\right] \end{aligned} \tag{11}$$

where an asterisk denotes the complex conjugate of a variable. The modal contribution given by the cross product $C_j(\overline{\omega}_i)C_k(\overline{\omega}_i)$ is much lower than the squared contribution of the jth mode as it is shown in the following section. This assumption is easily understood since these products involve the bridge transfer functions that reach a maximum value in the vicinity of the resonant frequencies and, then, decay rapidly. Thus, neglecting these terms, the total energy can be approximated with the expression:

$$E = \frac{c}{M}\sum_{i=1}^{M}\left[\sum_{j=1}^{N}|C_j(\overline{\omega}_i)|^2\right] \tag{12}$$

and, equivalently:

$$E = \frac{c}{M}\sum_{j=1}^{N}\left[\sum_{i=1}^{M}|C_j(\overline{\omega}_i)|^2\right] \tag{13}$$

Equation 13 states that the total harvested energy can be computed as the superposition of the modal contribution C_j, that is proportional to the instantaneous power related to each mode. This approach is advantageous since the railway bridge response is generally governed by the contribution of only a few modes of vibration.

2.2. The piezoelectric-mechanical coupled lumped parameter model

In this work, a cantilever bimorph beam with a tip mass M_t is considered (Figure 2) to assess the energy harvested from railway bridge vibration. The system is composed by two piezoelectric plates bonded to a brass substructure. The piezoelectrics are polarized in opposite directions along the plate thickness, and are connected in series. The system feeds a load resistance R_l. The beam dimensions are length L_s, width b, and the substructure and piezoelectric plates thicknesses are h_s and h_p, respectively. The material properties of both parts are defined by the Young's modulus (E_s and E_p) and the density (ρ_s and ρ_p).

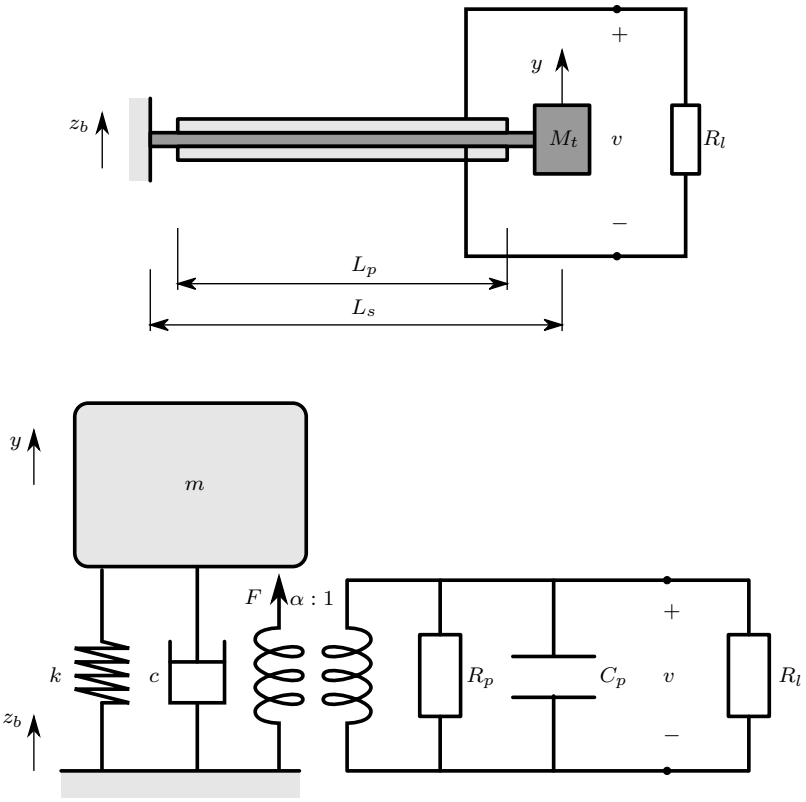

Figure 2: Cantilever bimorph beam and equivalent coupled lumped parameter model of a piezolectric energy harvester.

The lumped parameter model of the cantilever bimorph beam is defined by the equivalent mass per unit length $\overline{m}$ and the equivalent bending stiffness $\overline{EI}$ as is described in [35, 36]:

$$m = \frac{33}{140}\overline{m}L_s + M_t \qquad\qquad k = \frac{3\overline{EI}}{L_s^3} \tag{14}$$

where,

$$\overline{m} = b\left(2\rho_p h_p + \rho_s h_s\right) \tag{15}$$

$$\overline{I} = \frac{2b\left[\left(h_p + h_s/2\right)^3 - \left(h_s/2\right)^3\right]}{3} + \frac{bh_s^3}{12} \tag{16}$$

$$\overline{E} = \frac{E_p(2b\left[\left(h_p + h_s/2\right)^3 - \left(h_s/2\right)^3\right]/3) + E_s(bh_s^3/12)}{\overline{I}} \tag{17}$$

Moreover, an electromechanical coupling coefficient α, relating the electrical and mechanical energy, and the internal electrical capacitance C_p are defined for the bimorph beam [36]:

$$\alpha = \frac{b(h_s + h_p)}{2L_p} e_{31} \qquad\qquad C_p = \frac{bL_p}{2h_p}\epsilon_{33}^s \tag{18}$$

where e_{31} is the stress constant of the PZT material and ϵ_{33}^s its absolute permittivity. Also, an equivalent resistance R_{eq} can be computed from the load R_l and the piezoelectric leakage R_p resistances (Figure 2) in parallel.

Then, the governing equations of the piezoelectrically coupled lumped model are obtained from the equilibrium condition and the Kirchhoff laws applied to the system depicted in Figure 2 [34]:

$$\ddot{y}(t) + 2\zeta\omega\dot{y}(t) + \omega^2 y(t) - \frac{\alpha}{m}v(t) = -\kappa_1\ddot{z}_b(x,t) \tag{19}$$

$$C_p\dot{v}(t) + \frac{v(t)}{R_{eq}} + \alpha\dot{y}(t) = 0 \tag{20}$$

where v is the voltage output, ζ the mechanical damping ratio, ω the natural frequency of the device, and κ_1 a correction factor for the piezoelectrically coupled lumped model [37]. The correction factor takes into account the energy loss due to the error in predicting the natural frequency using the equivalent mass m and stiffness k given by Equation 14. The governing equations can be evaluated in terms of the amplitude and phase assuming a harmonic base excitation in the form $z_b(x,t) = z_0(x,\overline{\omega})\exp(\iota\overline{\omega}t)$:

$$(-\overline{\omega}^2 + 2\iota\overline{\omega}\zeta\omega + \omega^2)y_0(\overline{\omega}) - \frac{\alpha}{m}v_0(\overline{\omega}) = \kappa_1\overline{\omega}^2 z_0(x,\overline{\omega}) \tag{21}$$

$$\left(\iota\overline{\omega}C_p + \frac{1}{R_{eq}}\right)v_0(\overline{\omega}) + \iota\overline{\omega}\alpha y_0(\overline{\omega}) = 0 \tag{22}$$

The solution to the previous equations allows the computation of the displacement and voltage complex amplitudes of the beam:

$$y_0(\overline{\omega}) = \frac{\kappa_1\overline{\omega}^2 z_0(x,\overline{\omega})}{2\iota\overline{\omega}\zeta\omega + \omega^2 - \overline{\omega}^2 + \iota\overline{\omega}\alpha^2/m\left(\iota\overline{\omega}C_p + 1/R_{eq}\right)} \tag{23}$$

$$v_0(\overline{\omega}) = -\frac{\iota\overline{\omega}\alpha y_0(\overline{\omega})}{\left(\iota\overline{\omega}C_p + 1/R_{eq}\right)} \tag{24}$$

The instantaneous power becomes then $P_0(\overline{\omega}) = v_0^2(\overline{\omega})/R_l$ for the resistive load, and the harvested energy is obtained from power integration. Moreover, the bridge displacement in Equation 23 can be defined in terms of Equation 7 accounting for the jth modal contribution. Thus, Equation 23 stands for the modal contributions $y_j(\overline{\omega})$ and $v_j(\overline{\omega})$ to the system displacement and voltage, respectively. Therefore, the energy can be approximated similarly to Equation 13 considering the modal contribution to the instantaneous power $P_j(\overline{\omega}) = v_j^2(\overline{\omega})/R_l$:

$$E = \frac{1}{M}\sum_{j=1}^{N}\left[\sum_{i=1}^{M} P_j(\overline{\omega}_i)\right] \tag{25}$$

Then, Equation 25 allows to approximate the energy computation as the superposition of modal contributions to the instantaneous power. Next, this approximation is used for energy harvesting analysis in simply supported beams. The scope of the proposed method is later evaluated from experimental records measured in a real railway bridge from a High-Speed line.

3. Energy harvesting in simply supported beams

The equation of motion of a simply supported beam subjected to a moving load p travelling at constant speed V, under the assumptions of the Bernoulli-Euler theory, can be expressed as:

$$m_b\frac{\partial^2 z_b(x,t)}{\partial t^2} + c_b\frac{\partial z_b(x,t)}{\partial t} + E_bI_b\frac{\partial^4 z_b(x,t)}{\partial x^4} = p(x,t) \tag{26}$$

where,

$$p(x,t) = P_0\delta(x-Vt)\left[U(t) - U\left(t - \frac{L_b}{V}\right)\right] \tag{27}$$

and m_b and c_b are the bridge mass and damping per unit length, respectively, E_bI_b the bending stiffness, and L_b the span length. The force term is defined by the amplitude P_0, the Dirac delta $\delta(t)$ and the Heaviside $U(t)$ unit functions.

The bridge displacement is obtained by mode superposition according to Equation 7. The jth mode shape of a simply supported beam is expressed as $\phi_{bj}(x) = \sin(j\pi x/L_b)$ and the angular frequency is given by $\omega_{bj} = (j\pi)^2\sqrt{E_bI_b/m_bL_b^4}$. The generalised coordinate Z_{bj} is defined in terms of the transfer function H_{bj} and the moving load spectrum p_{bj} [38]:

$$H_{bj}(\overline{\omega}) = \frac{2L_b^3}{(j\pi)^4E_bI_b}\left[\frac{1}{(1-\beta_{bj}^2) + 2\iota\zeta_{bj}\beta_{bj}}\right] \tag{28}$$

$$p_{bj}(\overline{\omega}) = P_0\frac{\Omega_j}{\overline{\omega}^2 - \Omega_j^2}\left[(-1)^j\exp\left(\frac{-\iota j\pi\overline{\omega}}{\Omega_j}\right) - 1\right] \tag{29}$$

where $\beta_{bj} = \overline{\omega}/\omega_{bj}$ and $\Omega_j = j\pi V/L_b$ represent the dimensionless frequency and the forcing frequency, respectively. Then, the contribution of the jth mode to the harvested energy is fully defined by substituting the above expressions into Equations 13 and 25.

Following, the results of a sensitivity analysis are presented to determine the influence of: *i*) modal contributions, *ii*) maximum free vibration and cancellation phenomena, and *iii*) tuning effect on the harvested energy.

3.1. Sensitivity analysis

Bridges of lengths from 12.5 to 25 m in increments of 2.5 m are considered in this analysis covering usual short-to-medium span lengths prone to experience important vibration levels. The fundamental frequencies for each span are selected from the band prescribed by Eurocode 1 (EC1) [39] for the application of simplified methods, as the majority of existing simply supported bridges are expected to fall within these limits. Four evenly-spaced sample values between the lower and the upper frequency limits have been analysed (see Figure 3). These frequencies are referred to as $f_{1,000}$, $f_{1,035}$, $f_{1,075}$ and $f_{1,100}$. The linear mass for each length is adopted as $m_b = L_b \times 1000\,\mathrm{kg/m^2}$ [40]. Damping ratios prescribed by EC1 for pre-stressed concrete bridges as a function of the span length are assigned (see Figure 3). Each bridge is denoted by its span length and fundamental frequency, i.e., $[L_b = 17.5\,\mathrm{m};\ f_{1,035}]$.

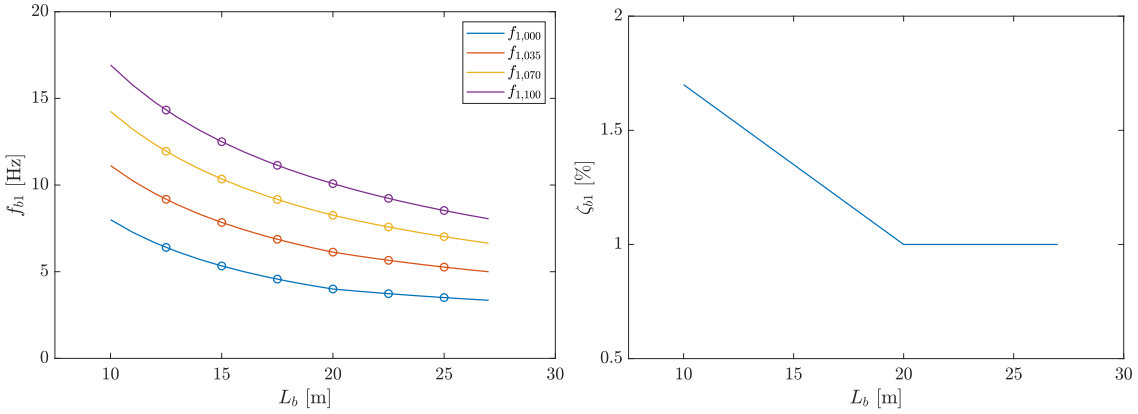

Figure 3: (a) EC1 lower and upper frequency limits for simplified dynamic analysis. Circles: Bridges under study. (b) Damping ratio according to EC1.

The energy harvester consists on two PZT-5A piezoelectric layers 50.8 mm × 31.8 mm bonded to a brass substructure as it is described in Figure 2. The system feeds a load resistance $R_l = 1\,\mathrm{k\Omega}$. The device is located in all the cases at $x = 0.35L_b$ to avoid points of zero amplitude of the first two mode shapes. The remaining properties are summarised in Table 1.

Table 1: Material and geometric properties of the energy harvester.

Property	Symbol	Value
Piezoelectric density	ρ_p [kg/m^3]	7800
Substructure density	ρ_s [kg/m^3]	9000
Piezoelectric Young's modulus	E_p [GPa]	66
Substructure Young's modulus	E_s [GPa]	105
Stress constant	e_{31} [C/m]	10.5
Vacuum permittivity	ϵ_0 [F/m]	8.854×10^{-12}
Absolute permittivity	ϵ_{33}^s [F/m]	$1500\epsilon_0$
Plate length	L_p [mm]	50.8
Plate width	b_p [mm]	31.8
Beam length	L_s [mm]	see Equation 30
Beam width	b_s [mm]	$b_s = b_p$
Piezoelectric thickness	h_p [mm]	0.26
Substructure thickness	h_s [mm]	0.14
Damping ratio	ζ [%]	2
Tip mass	M_t [kg]	see Equation 30
Leakage resistance	R_p [Ω]	5×10^9
Load resistance	R_l [Ω]	10^3
Correction factor	κ_1 [$-$]	1.0968

In the harvester tuning procedure the following is admitted: *i*) the natural frequency of the harvester matches the fundamental frequency of the bridge, ω_{b1}, and is calculated as $\sqrt{(k/m)}$, with k and m defined by Equation 14, and *ii*) the damping coefficient $c = 2\zeta\sqrt{km}$ of the harvester is the same for all the bridges. This last condition allows a comparable analysis of the energy harvesting for all the bridges according to Equation 13. This condition defines a constant value $r = km$. All the above allows the definition of the beam length and the tip mass in the tuning procedure for each bridge admitting the same cross section in all cases:

$$L_s = \sqrt[3]{\frac{3\overline{EI}}{\omega_{b1} r^{0.5}}} \qquad\qquad M_t = \frac{\sqrt[3]{r^2} - (33/140\overline{m})\sqrt[3]{3\overline{EI}\omega_{b1}^2}}{\omega_{b1}\sqrt[3]{r^{0.5}}} \tag{30}$$

Thus, the PZT plates (or the damping coefficient for the mechanical approach) do not change from one bridge to another and, therefore, it can be assumed that the energy performance only depends on the bridge and

the harvester dynamic behaviour. An analysis on the influence of parameter r on the harvester behaviour shows that, although the beam length decreases and the tip mass increases with increasing r (see Equation 30), the harvested energy does not vary since the damping coefficient does not change.

A representative value $r = 16\,\text{kgN/m}$ is estimated from the material and geometric properties of a bimorph beam of equal length as the piezolectric plates in Table 1 and a tip mass $M_t = 0.012\,\text{kg}$. This device is similar to those found in References [34, 36, 37]. Figure 4 shows the cantilever beam length L_s and the tip mass for the bridges of study. The beam length and the tip mass increase with the bridge span length to reach low natural frequencies, and are larger for the lowest frequency bands. The changes of slope in Figure 4 at $L_p = 20\,\text{m}$ are related with the fundamental frequency function prescribed by EC1. The beam length varies from 7.5 to 12 cm, and the tip mass takes values from 40 to 176 g depending on the bridge length and frequency band. Figure 4 can be used in the design of energy harvesters for railway bridges based on EC1 and under the assumptions adopted for the tuning procedure.

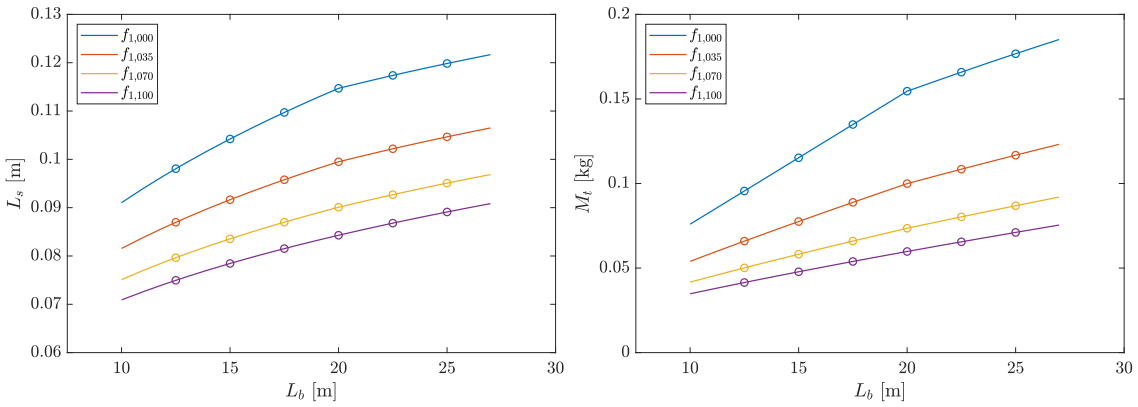

(a) (b)

Figure 4: (a) Cantilever beam lengths and (b) tip masses for bridges of study.

The harvested energy is obtained according to the mechanical approach presented in Section 2.1. The frequency step for this analysis is set to define the time span as $t_f = \kappa_t L_b/V$. Also, the maximum frequency is chosen to ensure a minimum time step $\Delta t = \min(2\pi/\kappa_\omega\omega_{b1},\, L_b/\kappa_v V)$ allowing a proper representation of the dynamic behaviour of the structure and the load excitation [40]. The values $\kappa_t = 8$, $\kappa_\omega = 60$ and $\kappa_v = 60$ are found to be optimum for this analysis.

As an example, Figure 5 shows the results for the bridge [$L_b = 17.5\,\text{m}$; $f_{1,035}$] and a moving load of amplitude $P_0 = 210\,\text{kN}$ travelling at $V = 250\,\text{km/h}$. The modal contribution to the mechanical energy shows maximum amplitude close to the bridge natural frequencies. The frequency content exhibits an undulatory behaviour throughout the frequency range alternating peaks and valleys each Ω_j due to the load spectrum defined by Equation 29. The maximum value of the modal contribution is reached for the

fundamental mode due to the tuning of the harvesting device to this frequency.

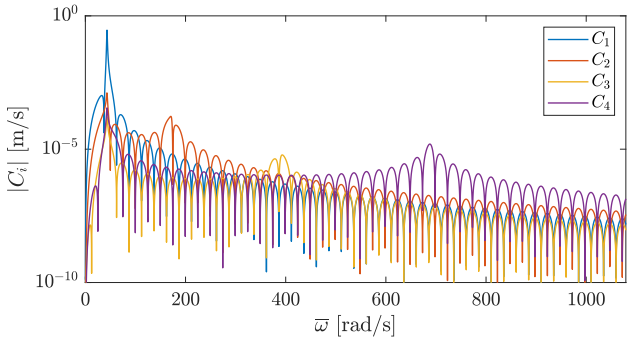

Figure 5: Modal energy contribution in the bridge [$L_b = 17.5\,\mathrm{m}$; $f_{1,035}$] due to a moving load travelling at $V = 250\,\mathrm{km/h}$.

This result confirms the assumptions adopted in the computation of the energy contributions in the previous section. It is clear that the product $C_j(\overline{\omega})C_k(\overline{\omega})$ in Equation 13 is lesser than $|C_j(\overline{\omega})|^2$, since it involves the product between transfer functions that reach maximum values in the vicinity of the natural frequencies (Figure 5). The harvested energy obtained from Equation 11 for $N = 10$ was $E = 4.36\,\mathrm{mJ}$, while the approximation given by Equation 13 is $4.35\,\mathrm{mJ}$. Therefore, the proposed approach for estimating the energy harvesting as modal superposition seems adequate. Furthermore, the contribution of the first mode of vibration exceeds 99% of the total energy. For this reason, in a first approach higher modal contributions are disregarded when the harvesting device is tuned to the first natural frequency of the bridge. In this case, the proposed procedure is simpler and is computationally efficient. Only the contribution of the fundamental mode will be considered in further analysis.

3.2. Maximum free vibration, cancellation phenomena and energy harvesting under a single moving load

In this section, energy harvesting is analysed in the simple case of a bridge traversed by a single load and the subsequent free vibration phase. In particular, the free vibration response of a beam after the passage of a single load has been analysed in the past as it is related with the amplification of the structure at resonance. When a resonant velocity coincides with a speed of maximum free vibration, an important amplification of the bridge response should be expected. On the contrary, if it is close to a cancellation condition, the resonant peak may become imperceptible [41]. Typically, the analytical solution for the maximum free vibration of a beam after de passage of a load at constant speed is expressed in terms of the non-dimensional speed $K_1 = \Omega_1/\omega_{b1} = \pi V/(\omega_{b1} L_b)$ and the amplification of the displacement R_1 referred to the static in the first mode of vibration. In the undamped case, the analytical relation between R_1 and K_1 is given by:

$$R_1 = \frac{K_1\sqrt{2}}{1-K_1^2}\sqrt{1-\cos\pi\cos\frac{\pi}{K_1}} \tag{31}$$

Figure 6.(a) (top) shows the analytical solution of R_1 and the results for bridges with span length $L_b = 17.5\,\text{m}$ and fundamental frequency indicated in Figure 3.(a). The analytical solution shows local maxima at $K_{1i}^m = [0.76\,, 0.26\,, 0.17\,, 0.13]$ that correspond to velocities leading to maximum free vibration, and zero displacement at the cancellation speeds $K_{1i}^c = [0.33\,, 0.20\,, 0.14\,, 0.11]$. The computed results for the four bridges of 17.5 m coincide with the analytical solution with just a small difference due to the presence of damping as referred in [40]. Figure 6.(b) (top) shows these results represented as the maximum displacement versus the load speed. The displacements in the case of the bridges with lower fundamental frequencies are higher than those with higher frequency for the same speed, due to their lower flexural stiffness. Equivalently, local maxima shift towards higher speeds as the frequency of the bridges increases.

The energy harvested under the single load passage (including the forced vibration phase in this case) shows a trend similar to that of the bridge, exhibiting successive maxima between cancellation speeds (see Figure 6.(a) (bottom)). The speeds for maximum and minimum energy levels are slightly lower than the speeds for maximum free vibration response and cancellation, K_{1n}^m and K_{1n}^c respectively, due to the harvester damping. This phenomenon is expected to happen under the passage of trains of several axle loads as well. The harvested energy decreases as the bridge frequency increases or, equivalently, as the bridge response is lower. The maximum energy is reached for higher speeds in the case of stiffer bridges following the tendency of the maximum bridge amplitude (Figure 6.(b) (bottom)).

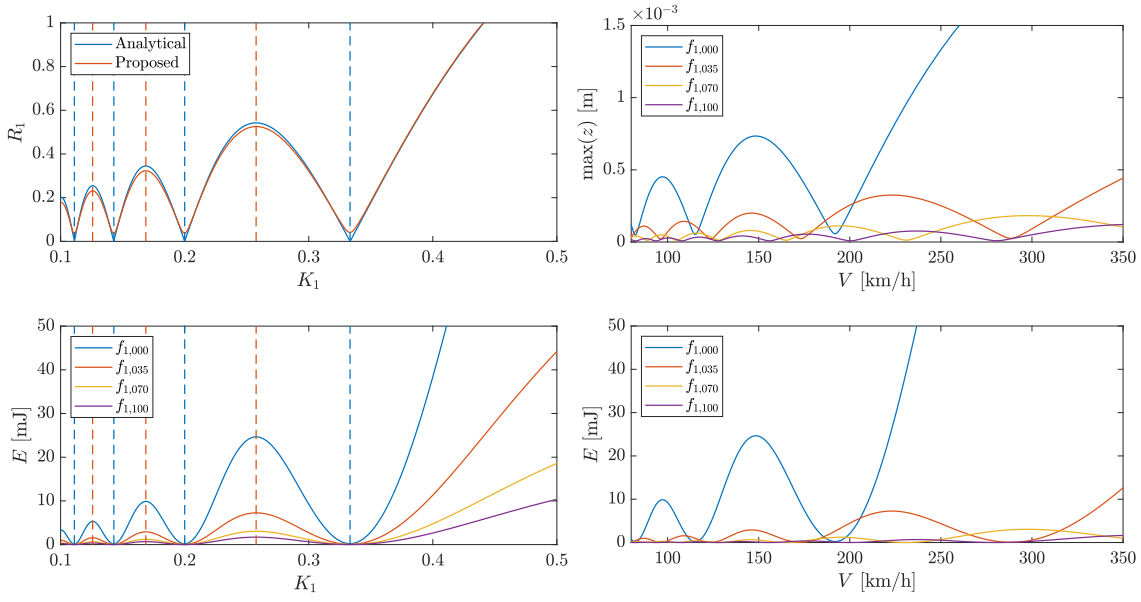

Figure 6: R_1 and maximum displacement in free vibration, and energy harvested at $x = 0.35L_b$ due to a moving load circulating in bridges of span length $L_b = 17.5\,\text{m}$ for different frequency bands vs. (a) K_1 and (b) load passage speed V. Maximum dynamic response and cancellation speeds are denoted by red and blue dashed lines, respectively.

Similarly, the dynamic response of the bridge decreases as the span length increases for a fixed frequency band, as can be seen in Figure 7. Moreover, the maximum dynamic and cancellation speeds are higher for the longest bridges. The same behaviour is observed in the energy harvested. Therefore, it is expected that the energy harvesting in bridges of the same span length will be lower for increasing stiffness in the current range of commercial speeds. Also, the energy harvested will decrease as the span length increases for the same frequency band.

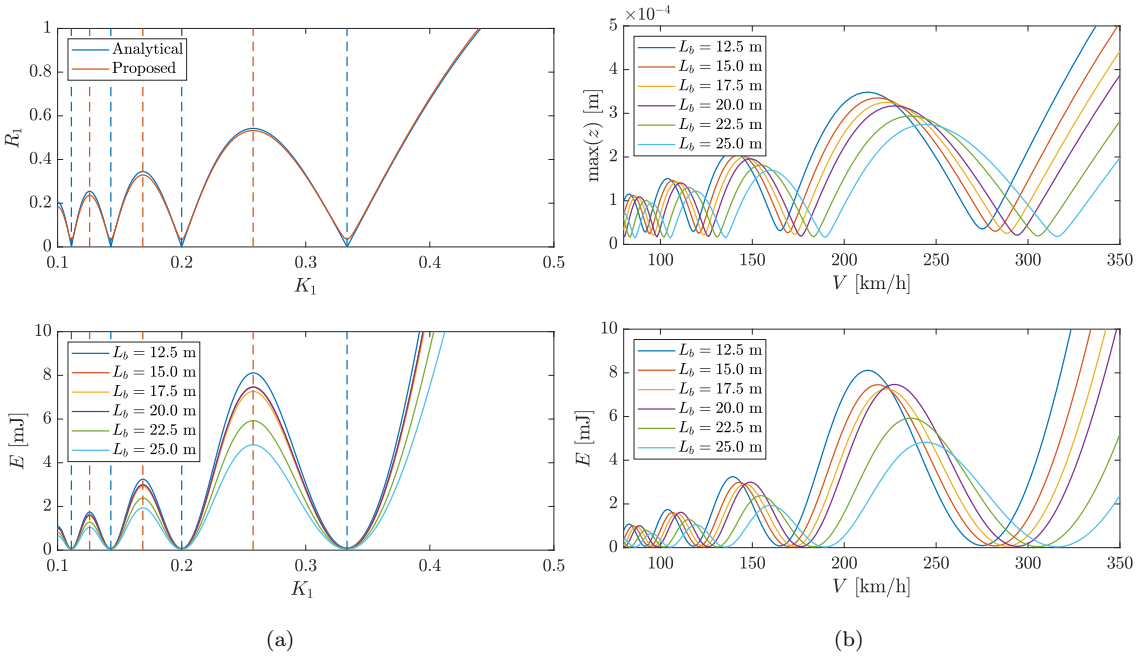

(a) (b)

Figure 7: R_1 and maximum displacement in free vibration, and energy harvested at $x = 0.35L_b$ due to a moving load circulating in bridges of different span length with natural frequency $f_{1,035}$ vs. (a) K_1 and (b) load passage speed. Maximum dynamic response and cancellation speeds are denoted either by red and blue dashed lines, respectively.

Once the dynamic behaviour of the bridge and the energy harvesting have been investigated, two additional conditions are studied: the energy loss in detuned systems and the effect of tuning the harvester to a higher bridge frequency. This analysis is limited to a bridge of span length $L_b = 17.5\,\text{m}$ and natural frequency $f_{1,035}$.

Figure 8.(a) shows the detuning effect as a reduction of the natural frequency of the harvesting device with respect to the fundamental frequency of the bridge. The harvested energy is drastically reduced as a result of the detuning. Also, the speeds for maximum and minimum harvested energy are slightly reduced with respect to K_{1i}^m and K_{1i}^c. This result highlights both the importance of adequately identifying the bridge dynamic properties and, subsequently, the correct tuning of the harvesting device. On the other hand, further studies show that the effect of tuning to the bridge natural frequency instead of the resonance frequency does not significantly affect the harvested energy, since these structures are slightly damped.

The energy harvested by two different devices tuned to the natural frequencies of the first and second modes of the bridge is shown in Figure 8.(b). The device location remains at $x = 0.35L_b$. The energy harvested by the systems tuned to the second natural frequency is considerably lower than in the case previously studied due to the lower contribution of the second mode. Similar results are obtained for systems tuned to higher frequencies. Therefore, it can be concluded that the harvesting devices should be paired to the fundamental frequency of the bridge and, consequently, would be most effective close to mid-span in simply-supported bridges where the modal amplitude reaches its maximum value. This configuration is chosen in following sections.

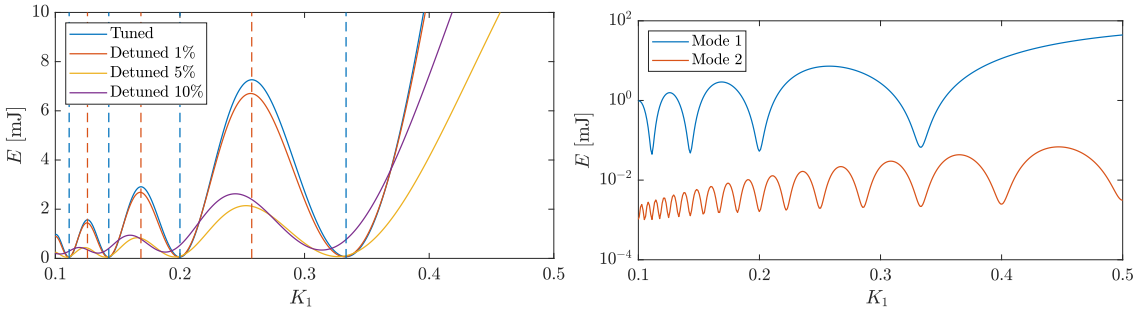

(a) (b)

Figure 8: Tuning effect on energy harvesting in a bridge [$L_b = 17.5\,\mathrm{m}$; $f_{1,035}$] at $x = 0.35L_b$. (a) Energy harvested by a detuned device to the first natural frequency. Maximum dynamic response and cancellation speeds are denoted either by red and blue dashed lines, respectively. (b) Energy harvested by a tuned device to the second mode frequency.

3.3. Energy harvesting under trains of moving loads

This section studies the energy harvesting during a train passage according the coupled approach presented in Section 2.2. The HSLM-A universal train model defined in EC1 is considered in what follows. This family of trains are used to evaluate the dynamic effects induced in HSL bridges by European commercial trains. In this sense, the analysis presented in this section allows a characterization of the available energy in high-speed bridges during the train passages. The HSLM-A trains have different number and length of carriages, bogie distances and axle loads. Table 2 shows a scheme of the train load and the properties for each type of train.

The trains are described by the axle loads P_k and their geometrical distribution. The modal load $p_{bj}^{tr}(\overline{\omega})$ can be computed as the superposition of L single loads given by Equation 29, with a time shift t_k defined by the axle position:

$$p_{bj}^{tr}(\overline{\omega}) = \sum_{k=1}^{L} \left[p_{bj}(P_k, \overline{\omega}) \exp\left(-\iota \overline{\omega} t_k\right) \right] \tag{32}$$

Table 2: Definition of HSLM train series.

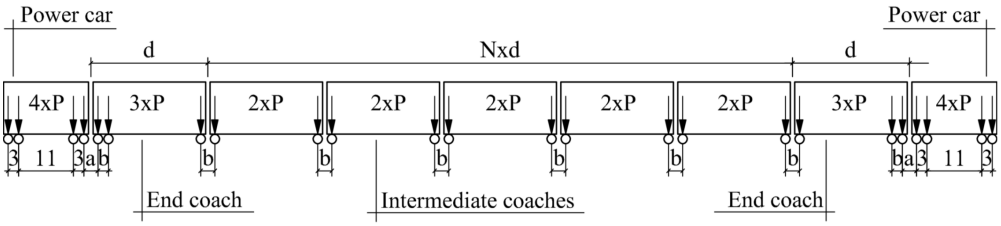

Train name	N	a [m]	d [m]	b [m]	P [kN]
HSLM-A1	18	3.525	18	2.0	170
HSLM-A2	17	3.525	19	3.5	200
HSLM-A3	16	3.525	20	2.0	180
HSLM-A4	15	3.525	21	3.0	190
HSLM-A5	14	3.525	22	2.0	170
HSLM-A6	13	3.525	23	2.0	180
HSLM-A7	13	3.525	24	2.0	190
HSLM-A8	12	3.525	25	2.5	190
HSLM-A9	11	3.525	26	2.0	210
HSLM-A10	11	3.525	27	2.0	210

The maximum bridge response due to a train passage depends both on the periodicity of the loads and on the amplitude of the free vibrations induced by each single axle, as referred in [40, 41]. It is well known that the successive passage of equally spaced loads can cause a resonant behaviour of the bridge when the train speed is $V_{jn}^r = \omega_{bj} d/(2\pi n)$, where j corresponds to the excited frequency and n is the number of cycles between loads pass in free vibration or, equivalently, a non-dimensional resonance speed can be defined as $K_{jn}^r = jd/(2L_b n)$. The amplitude at resonance is related with the level of free vibration caused by a single moving load at the resonant velocity. The amplitude will be very amplified when the non-dimensional resonance speed matches one of the local maxima K_{1i}^m and may become imperceptible at a cancellation speed K_{1i}^c.

Figure 9 shows curves of non-dimensional resonance speeds K_{1n}^r $(n = 1, \dots 4)$ as a function of the ratio L_b/d. Each curve represents the dimensionless speed at which resonance of the fundamental mode occurs for a bridge span length L_b and a characteristic distance d. The velocities for maximum free vibration K_{1i}^m and cancellation K_{1i}^c are marked in dashed red and blue lines, respectively. As an example, the resonance speeds for the HSLM train series are marked in black asterisks for the bridge $[L_b = 17.50\,\text{m};\, f_{1,035}]$, that can be read from left to right for trains HSLM-A1 to HSLM-A10 according to the increasing car length (see Table 2).

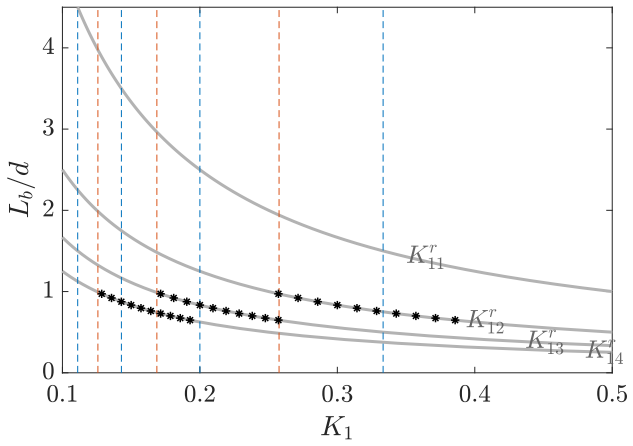

Figure 9: Non-dimensional resonance speed curves K_{1n}^r. Maximum dynamic response and cancellation speeds are denoted by red and blue dashed lines, respectively. Resonance speeds for HSLM series are marked in black asterisks for bridges of length $L_b = 17.50\,\mathrm{m}$.

Only resonance speeds corresponding to $n > 1$ are indicated in order to represent realistic velocities (note that $K_1 = 0.5$ corresponds to 432.8 km/h for this bridge). Also, note that the non-dimensional resonance speed does not depend on the natural frequency of the bridge and, therefore, this representation is valid for all bridges with span length $L_b = 17.50\,\mathrm{m}$.

The energy harvesting is investigated in two cases selected from the representation of the resonance speed curves: *i*) HSLM-A1 passage at the resonance speed $V_{12}^r = 222.6\,\mathrm{km/h}$ ($K_{12}^r = 0.2571$) and *ii*) HSLM-A6 passage at $V_{12}^r = 284.4\,\mathrm{km/h}$ ($K_{12}^r = 0.3286$). The first case is close to the point K_{12}^m of maximum amplitude in free vibration, whereas the second case almost matches the first cancellation at K_{11}^c. These conditions should produce a maximum resonance and the cancellation of resonance in the bridge response. The harvester device is tuned to the fundamental frequency of the bridge and is located at midspan.

Figure 10 and Figure 11 show the computed results in both cases. The frequency content of the acceleration shows a main peak at the resonance frequency of the fundamental mode. The difference in amplitudes is justified by the conditions of maximum and cancellation of resonance, respectively. Moreover, the frequency content shows peaks at the bogie passage frequency given by V/d (3.4 Hz in both cases), and its related high-order harmonics. No additional peaks are found since only the contribution of the first mode is considered. The time history also shows two very different behaviours: a strong resonance in the first case in comparison to the second case, where no amplification is detected under each successive bogie passage. The harvesting device is highly excited due to the tuning effect to the fundamental frequency, and its maximum acceleration is found to be much higher than the bridge response.

The voltage exhibits a similar behaviour to the harvester response reaching a maximum of 4.5 V due to the HSLM-A1 passage and 0.5 V in the second case. The time period T used to compute the harvested

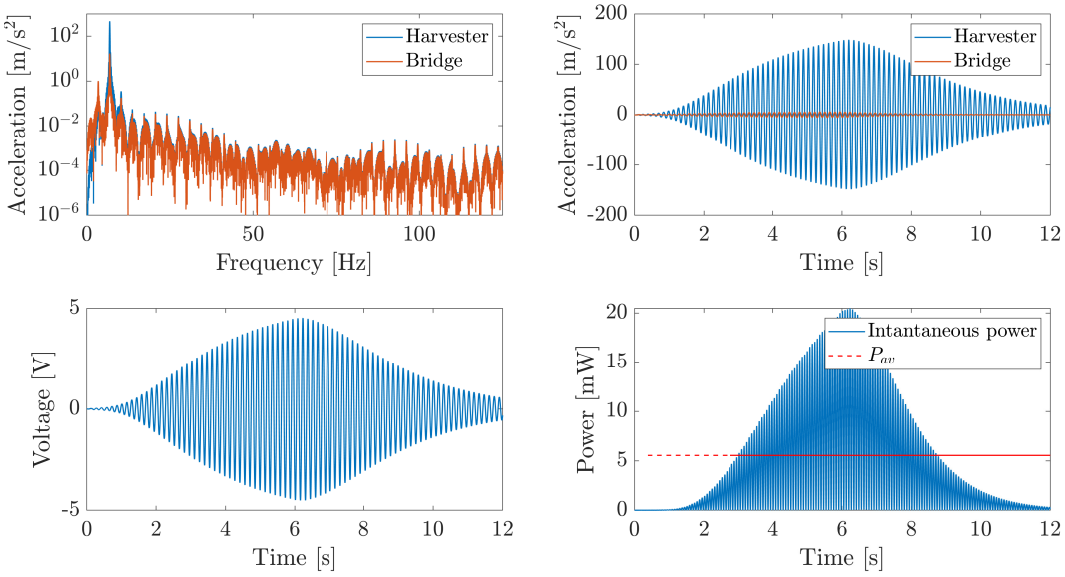

Figure 10: Bridge and harvester vertical acceleration, voltage and normalised power under HSLM-A1 train passage travelling at $V = 222.6\,\text{km/h}$ [$L_b = 17.50\,\text{m}$; $f_{1,035}$].

energy is set to the part of the instantaneous power with a significant level. The standard DIN 45672 [42] is used to fix the time period T as the part of the signal where the root mean square value exceeds a noise level defined by a heuristic algorithm. The instantaneous power and the average power computed as $P_{av} = E/T$ in the time period T are shown in Figure 10. The total energy reaches 139.3 mJ and the average power 5.54 mW for the first case. The energy and the average power are drastically reduced to 1.2 mJ and 0.05 mW in the second case when the resonance is cancelled.

Any modification of the train speed defines new points in Figure 9 according to the dimensionless speed K_1 with a constant L_b/d ratio. The new points do not necessarily belong to a resonance velocity curve K_{1n}^r. In that case, the bridge response is expected to be lower than in the resonance regime as well as the energy harvested. The energy and the average power due to the HSLM-A1 passage at $K_1 = 0.3$ ($V = 259.7\,\text{km/h}$) decreases to $E = 0.87\,\text{mJ}$ and $P_{av} = 0.035\,\text{mW}$. The computed results for the HSLM-A6 at the same dimensionless speed are $E = 2.77\,\text{mJ}$ and $P_{av} = 0.110\,\text{mW}$, slightly higher than at cancellation of the resonance. These results emphasize the need to understand the influence of the bridge dynamic behaviour on energy harvesting.

Figure 12 summarises the computed results for maximum bridge acceleration and harvested energy in the non-dimensionless speed range from 0.1 to 0.5 for all trains of the HSLM series. Two types of plots are represented: *i*) maximum acceleration and energy versus the non-dimensionless speed, and *ii*) a contour map of those quantities as a function of L_b/d and K_1. The second type of plot is complementary to Figure

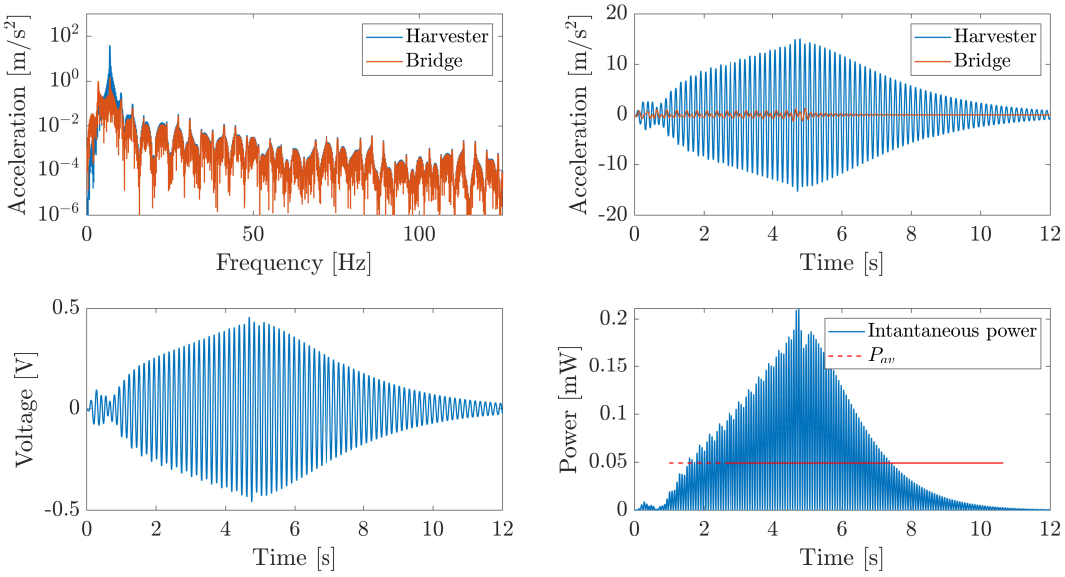

Figure 11: Bridge and harvester vertical acceleration, voltage and normalised power under HSLM-A6 train passage travelling at $V = 284.4\,\text{km/h}$ [$L_b = 17.50\,\text{m}$; $f_{1,035}$].

9, with the same meaning of lines but with a different range of L_b/d. The maximum accelerations are found between the cancellation speeds with amplifications close to the resonance speeds. Local maxima are not observed when the resonance velocity coincides with cancellation, as occurred with the HSLM-A6 train travelling at $K_{12}^r = 0.3286$. The harvested energy shows a similar pattern but the levels collected around the resonance velocities are much higher than at other velocities. This behaviour is due to the tuning effect of the harvester device to the fundamental frequency that highly amplifies the bridge response as shown in Figure 10 and Figure 11. This effect is also observed in the contour map in Figure 12, where the maximum harvested energy is obtained around the resonance curves described in Figure 9.

The results for all the bridges shown in Figure 3 are studied to investigate the available energy in railway bridges due to train passage. The total number of analysed cases is 84.000 (6 bridge lengths, 4 frequency bands, 10 train types and 350 passages in the non-dimensionless speed range from 0.1 to 0.5). Figure 13 shows the harvested energy superimposed for all the cases versus K_1. Although the vast number of cases makes the analysis difficult, it can be observed that the results follow a similar trend to the previous studies. The maximum energy is found around the maximum dynamic response speeds and is close to zero at the cancellation speeds. The energy values may be described by a normal distribution with mean $\mu = 115.696\,\text{mJ}$ and standard deviation $\sigma = 658.193\,\text{mJ}$ in the complete speed range. The high standard deviation is related to the dynamic behaviour of the bridge-harvester system depending on the load speed. The analysis of the harvested energy below K_{11}^c resulted in $[\mu, \sigma] = [2.970, 15.385]\,\text{mJ}$ which could be more relevant for

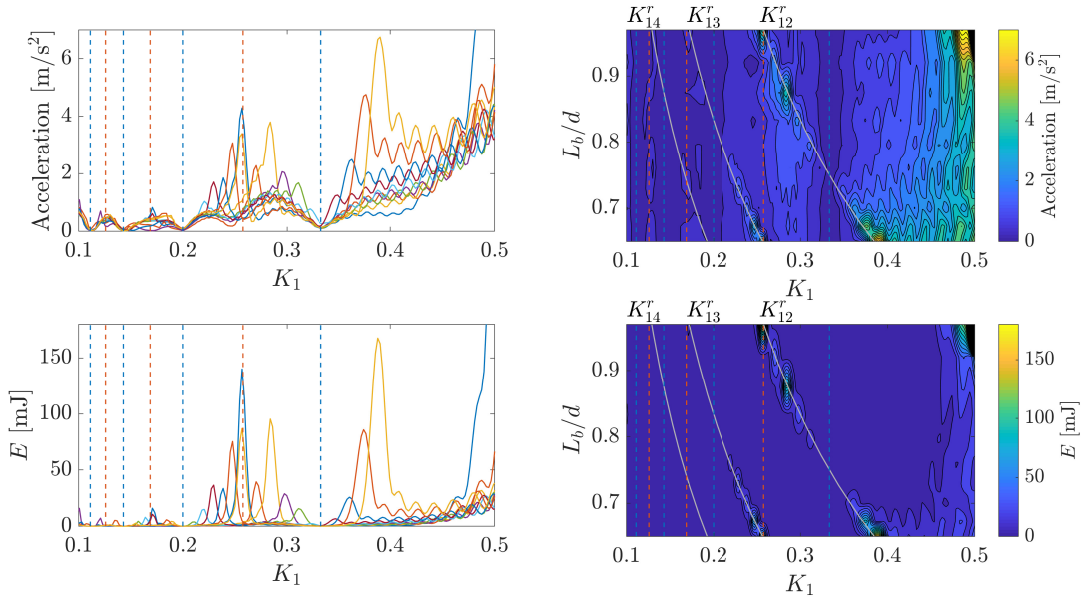

Figure 12: Maximum bridge acceleration and energy harvesting due to HSLM train passages at $x = 0.5L_b$ [$L_b = 17.50\,\mathrm{m}$; $f_{1,035}$]. Maximum dynamic response and cancellation speeds are denoted by red and blue dashed lines, respectively.

commercial speeds in current railway lines.

Moreover, Table 3 summarises the normal distribution of the energy at resonance speeds K_{1n}^r (corresponding to cases belonging to the resonance curves in Figure 9), the maximum dynamic speed K_{1i}^m, and the cancellation speeds K_{1i}^c for all the cases. From these results, it can be concluded that the maximum available energy in the bridge dynamic response is due to trains travelling close to a resonance speed far from a cancellation condition and the energy levels are much lower in other cases.

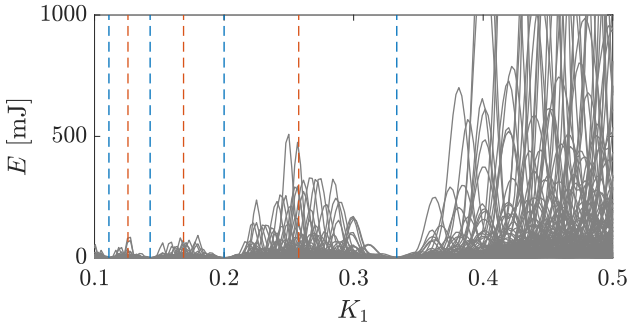

Figure 13: Energy harvesting due to HSLM train passages at $x = 0.5L_b$ for all bridges. Maximum dynamic response and cancellation speeds are denoted red and blue dashed lines, respectively.

Table 3: Mean and standard deviation of energy harvesting from HSLM-A passage in different conditions.

	K_{12}^r	K_{13}^r	K_{14}^r	K_{12}^m	K_{13}^m	K_{14}^m	K_{11}^c	K_{12}^c	K_{13}^c	K_{14}^c
μ [mJ]	24.51	4.03	1.38	14.94	2.76	1.76	0.12	0.05	0.05	0.07
σ [mJ]	137.96	18.73	5.94	46.52	8.06	7.43	0.23	0.08	0.09	0.13

4. Case study

Next, the possibility of energy harvesting is analysed from experimental records of a real bridge to support the conclusions of previous sections. The authors performed an experimental campaign on several railway bridges, including the identification of the bridge modal parameters and the recording of vibration levels under operational conditions [43]. A portable acquisition system Brüel & Kjaer LAN-XI and Endevco model 86 piezoelectric accelerometers were used in the experimental tests (Figure 14). Measurements were filtered to carry out data analysis in the frequency range of interest ($0 - 30$ Hz). The modal parameters of the bridges were identified from ambient vibration data by the stochastic subspace identification technique [44]. The vertical response of the structure was recorded under the circulation of passenger trains crossing the bridge at different speeds.

Jabalón HSL Bridge (Figure 14) is selected from the experimental campaign. This bridge is composed by three identical simply supported bays of equal span lengths $L_b = 24$ m. The structure crosses Jabalón River with a 134° skew angle. Each deck consists of a cast-in-situ concrete slab with dimensions 11.6 m × 0.3 m (width × thickness). The slab rests over five prestressed concrete I girders with a height of 2.05 m separated 2.625 m. The girders lean on the supports through laminated rubber bearings. The slab carries two ballasted tracks with UIC gauge (1435 mm), UIC60 rails and mono-block concrete sleepers every 0.60 m. Figure 14 shows the measurement points, all of them located at span 1. The fundamental mode corresponds to the first longitudinal bending mode shape with natural frequency 6.3 Hz and modal damping 3.2 %. 20 passenger trains circulations were recorded on May 8th 2019 between 11.52 and 15.24 hours. All the trains were RENFE High-Speed services, and the identified travelling velocities, average axle loads of the passenger coaches and the circulating track are included in Table 4. More details can be found in Reference [43].

The bridge response is used as the input in the coupled model described in Section 2.2. The right-hand side of Equation 23 concerning the frequency content of the bridge acceleration is obtained by Fourier transform of the recorded vibrations. The harvester properties adopted are the same as in the previous section, and the device is tuned to the bridge fundamental frequency. The energy harvested in the load resistance is obtained once the system of equations has been solved in the frequency range. Table 4 shows the energy and average power obtained from the bridge response at accelerometer 7 for all train passages (see Figure 14). The dimensionless speed is shown as a reference.

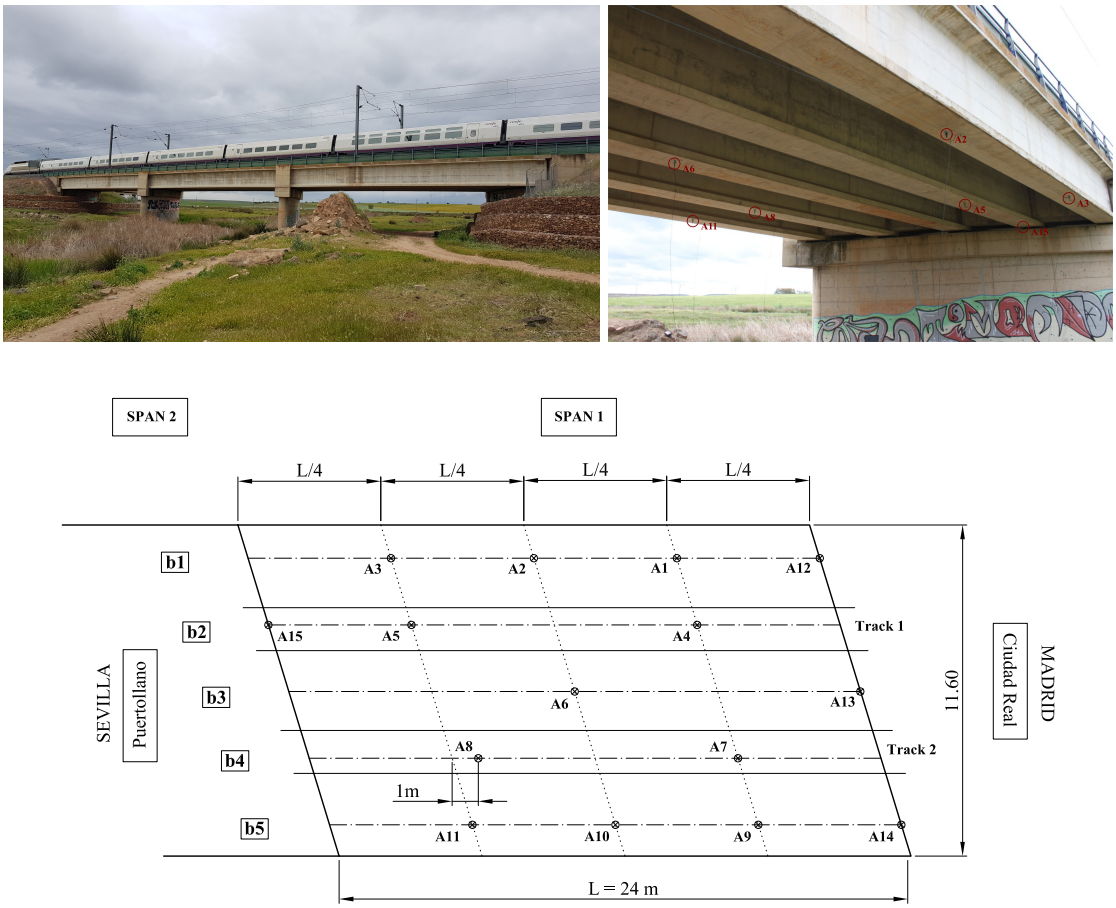

Figure 14: HSL bridge over Jabalón River (38°53'51.3"N 3°57'53.0"W), location of the sensors and experimental setup.

The energy levels vary in a wide range from almost zero to 0.84 mJ for train passage #9. Two circulations are analysed to bring out these differences in the harvested energy. Passage #3 is one of the almost zero energy circulations, corresponding to a Renfe S104 train travelling on track 2 at $V = 251$ km/h. Figure 15 shows the experimental bridge and harvester accelerations, voltage and instantaneous power induced by this train. The harvester acceleration is similar to the bridge acceleration (Figure 15). The frequency content of the acceleration shows little amplification of the bridge response around the first natural frequency, meaning that the fundamental mode was not excited during the train passage. The frequency content of the harvester acceleration is almost identical to that of the bridge for frequencies higher that 10 Hz. This behaviour causes that the harvester is not properly excited by the bridge vibration. Consequently, the energy levels are almost zero since the harvester deformation is very small. The voltage across the resistor is around two volts, and the average power below one milliwatt.

On the other hand, a Renfe S102 train circulating on the same track at $V = 274$ km/h (passage #11) leads to a high energy level. In this case, the frequency content of the bridge acceleration is mainly found

Table 4: Train passages recorded at Jabalón HSL Bridge.

Passage	Train	Track	V [km/h]	K_1	P_k [kN]	E [mJ]	P_{av} [mW]
1	S102	1	290	0.27	165	0.18	0.0082
2	S102	2	266	0.24	165	0.03	0.0011
3	S104	2	251	0.23	153	0.00	0.0001
4	S112-Duplex	1	267	0.25	172	0.46	0.0184
5	S102	1	240	0.22	165	0.01	0.0002
6	S102-Duplex	2	263	0.24	165	0.64	0.0253
7	S100	1	290	0.27	156	0.02	0.0008
8	S112	1	269	0.25	172	0.18	0.0080
9	S102-Duplex	2	265	0.24	165	0.84	0.0334
10	S130	1	236	0.22	165	0.01	0.0003
11	S102	2	274	0.25	165	0.35	0.0151
12	S102-Duplex	1	267	0.25	165	0.44	0.0175
13	S130	2	237	0.22	165	0.02	0.0010
14	S104	1	249	0.23	153	0.00	0
15	S100	2	262	0.24	156	0.04	0.0015
16	S130	1	236	0.22	165	0.01	0.0002
17	S100	1	290	0.27	156	0.02	0.0007
18	S102	2	273	0.25	165	0.35	0.0148
19	S104	1	255	0.23	153	0.00	0
20	S104	2	236	0.22	153	0.00	0.0001

around the fundamental frequency to which the harvester is tuned. The system response is highly amplified exhibiting a resonant behaviour, as it is also observed in the voltage and power time histories. The maximum acceleration level of the harvester reaches $10\,\mathrm{m/s^2}$, the maximum voltage $0.35\,\mathrm{V}$ and the average power $0.0151\,\mathrm{mW}$. This behaviour can be considered as optimal performance of the harvester.

Consistent results are obtained for the rest of the train passages. The maximum harvested energy is obtained from duplex configurations in comparison to simple configurations of the trains. There is not a clear influence of the circulating track or the train speed on the energy levels. The total energy harvested by the system is $3.6\,\mathrm{mJ}$ for 20 train passages in the measurement time of approximately three and a half hours.

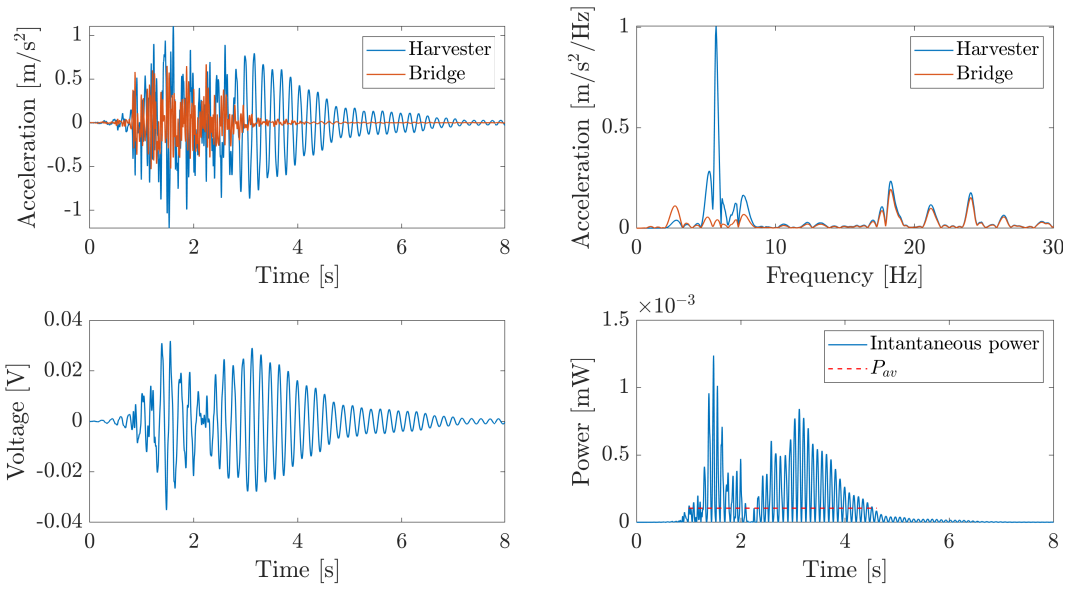

Figure 15: Bridge and harvester acceleration, voltage and power at point 7 induced by Renfe S104 train circulating on track 2 at $V = 251\,\text{km/h}$ (passage #3).

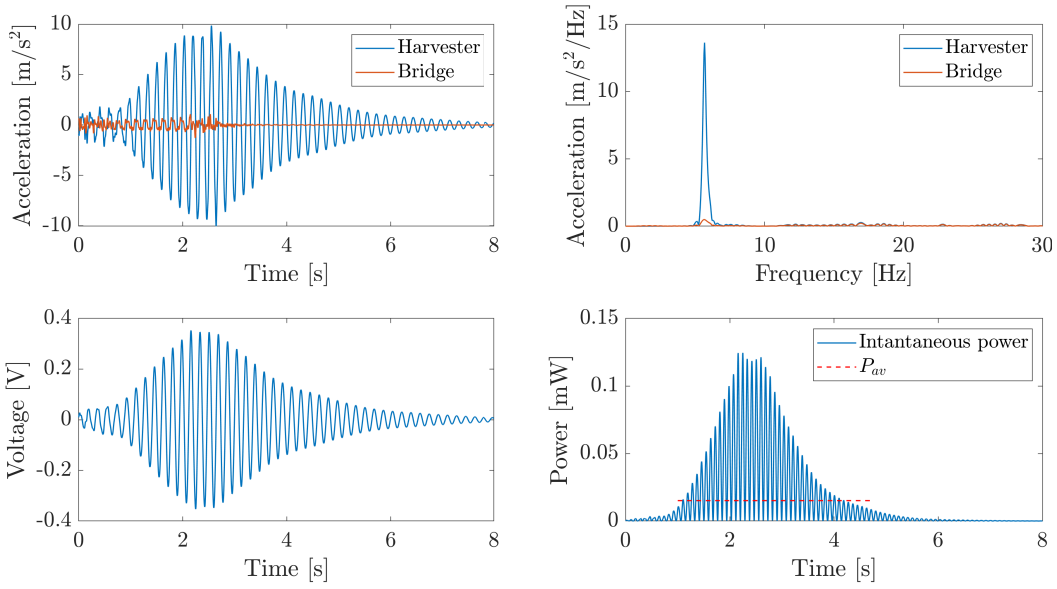

Figure 16: Bridge and harvester acceleration, voltage and power at point 7 induced by Renfe S102 train circulating on track 2 at $V = 274\,\text{km/h}$ (passage #11).

5. Conclusions

The aim of this research is the analysis of energy harvesting performance in railway bridges, taking into account the influence of the bridge dynamic behaviour under different train circulating conditions. This research includes both a theoretical analysis of simply-supported beams and the experimental application using the acceleration data on a real bridge from the Madrid-Sevilla HSL.

The theoretical analysis to compute the energy harvested by the train load passage is based on a modal superposition approach. This approximation allows computing the energy as the sum of modal contributions. The fundamental mode contribution is found to be much larger than the related to higher-order frequencies. The results of this analysis show that the energy harvesting performance is very related to the bridge dynamic behaviour under train passages. The influence of maximum dynamic response and cancellation condition is studied in the harvested energy under a single moving load. The maximum and minimum harvested energy are found at passage speeds related to these two phenomena. This conclusion is also applicable to the energy harvested from train-induced vibrations.

The amount of harvested energy depends on the intensity of the rail traffic and the design of the harvester. In this work, a device with fixed design parameters has been considered to obtain comparable energy levels in the studied bridges. The conclusions drawn from the experimental case study show that the harvested energy in three and a half hours and 20 train passages could have been 3.6 mJ. This result is similar to other energy scavenge investigations in bridges [13, 26] but lower than previous studies in which the harvester device is attached to the railway track where the vibration is higher [17]. Although the available power is small, this energy source can be used in intermittent storage and measurement operations. The amount of energy can be increased using several harvesters according to the output required power of a monitoring system. Then, it is expected that the results of this analysis could be helpful for energy harvesting applications on railway bridges to feed low power consumption devices, nodes, and sensors of monitoring systems in remote areas, and also for the development of harvesters as direct structural health monitoring devices [27, 28].

Acknowledgements

The authors would like to acknowledge the financial support provided by the Spanish Ministries of Economy and Competitiveness, Science and Innovation under research projects BIA2016-75042-C2 and PID2019-109622RB; US-126491 funded by the FEDER Andalucía 2014-2020 Operational Program; Generalitat Valenciana under research project [AICO2019/175] and the Andalusian Scientific Computing Centre (CICA).

References

[1] European Commission, Communication from the commission concerning the development of a Single European Railway Area, Tech. rep. (2010).

[2] European Commission, Transport in the European Union. Current Trends and Issues, Tech. rep. (March 2019).

[3] L. Frýba, Dynamic behaviour of bridges due to high-speed trains, in: Bridges for High-Speed Railways, CR Press, London, (2008) 137–158.

[4] W. Hoorpah, Dynamic calculations of high-speed railway bridges in france – some case studies, in: Dynamics of High-Speed Railway Bridges, CR Press, London, (2008) 133–145.

[5] M. Zacher, M. Baeßler, Dynamic behaviour of ballast on railway bridges, in: Dynamics of High-Speed Railway Bridges, CR Press, (London) 2008, 99–112.

[6] A. Romero, M. Solís, J. Domínguez, P. Galvín, Soil–structure interaction in resonant railway bridges, Soil Dynamics and Earthquake Engineering 47 (2013) 108 – 116, sI: José Manuel Roësset.

[7] G. De Roeck, The state-of-the-art of damage detection by vibration monitoring: The SIMCES experience, Journal of Structural Control 10 (2) (2003) 127–134

[8] D. Barke, K.W. Chiu, Structural health monitoring in the railway industry: A review, Structural Health Monitoring 4 (1) (2005) 81–94

[9] M. Vagnoli, R. Remenyte-Prescott, J. Andrews, Railway bridge structural health monitoring and fault detection: State-of-the-art methods and future challenges, Structural Health Monitoring 17 (4) (2018) 971–1007

[10] C. Wei, X. Jing, A comprehensive review on vibration energy harvesting: Modelling and realization, Renewable and Sustainable Energy Reviews 74 (2017) 1–18

[11] T. Yildirim, M.H. Ghayesh, W. Li, G. Alici, A review on performance enhancement techniques for ambient vibration energy harvesters, Renewable and Sustainable Energy Reviews 71 (2017) 435–449

[12] M.R. Sarker, S. Julai, M.F.M Sabri, S.M. Said, M.M. Islam, M. Tahir, Review of piezoelectric energy harvesting system and application of optimization techniques to enhance the performance of the harvesting system, Sensors and Actuators, A: Physical 300 (2019) 111634

[13] M. Peigney, D. Siegert, Piezoelectric energy harvesting from traffic-induced bridge vibrations, Smart Materials and Structures 22 (9).

[14] J.J. Wang, G.P. Penamalli, L. Zuo, Electromagnetic energy harvesting from train induced railway track vibrations, Proceedings of 2012 8th IEEE/ASME International Conference on Mechatronic and Embedded Systems and Applications, MESA (2012) 29–34

[15] A. Pourghodrat, C.A. Nelson, S.E. Hansen, V. Kamarajugadda, S.R. Platt, Power harvesting systems design for railroad safety, Proceedings of the Institution of Mechanical Engineers, Part F: Journal of Rail and Rapid Transit 228 (5) (2014) 504–521

[16] W. Hou, Y. Li, W. Guo, J. Li, Y. Chen, X. Duan, Railway vehicle induced vibration energy harvesting and saving of rail transit segmental prefabricated and assembling bridges, Journal of Cleaner Production 182 (2018) 946–959

[17] C.A. Nelson, S.R. Platt, D. Albrecht, V. Kamarajugadda, M. Fateh, Power harvesting for railroad track health monitoring using piezoelectric and inductive devices, Proceedings of SPIE - The International Society for Optical Engineering 6928 (2008) 69280R

[18] Y. Tianchen, Y. Jian, S. Ruigang, L. Xiaowei, Vibration energy harvesting system for railroad safety based on running vehicles, Smart Materials and Structures 23 (12) (2014) 125046

[19] A. Erturk, D.J. Inman, Broadband piezoelectric power generation on high-energy orbits of the bistable duffing oscillator with electromechanical coupling, Journal of Sound and Vibration 330 (10) (2011) 2339–2353

[20] S. Ali, M. Friswell, S. Adhikari, Analysis of energy harvesters for highway bridges, Journal of Intelligent Material Systems and Structures 22 (16) (2011) 1929–1938.

[21] G. Gatti, M.J. Brennan, M.G. Tehrani, D.J. Thompson, Harvesting energy from the vibration of a passing train using a single-degree-of-freedom oscillator, Mechanical Systems and Signal Processing 66-67 (2016) 785–792

[22] D.R.M. Milne, L.M. Le Pen, D.J. Thompson, W. Powrie, Properties of train load frequencies and their applications, Journal of Sound and Vibration 397 (2017) 123 – 140.

[23] V.G. Cleante, M.J. Brennan, G. Gatti, D.J. Thompson, On the target frequency for harvesting energy from track vibrations due to passing trains, Mechanical Systems and Signal Processing 114 (2019) 212–223

[24] P. Cahill, N.A.N. Nuallain, N. Jackson, A. Mathewson, R. Karoumi, V. Pakrashi, Energy harvesting from train-induced response in bridges, Journal of Bridge Engineering 19 (9) (2014) 04014034

[25] P. Cahill, V. Jaksic, J. Keane, A. O'Sullivan, A. Mathewson, S. Ali, V. Pakrashi, Effect of road surface, vehicle, and device characteristics on energy harvesting from bridge–vehicle interactions, Computer-Aided Civil and Infrastructure Engineering 31 (12) (2016) 921–935.

[26] P. Cahill, A. Mathewson, V. Pakrashi, Experimental validation of piezoelectric energy-harvesting device for built infrastructure applications, Journal of Bridge Engineering 23 (8).

[27] P. Cahill, B. Hazra, R. Karoumi, A. Mathewson, V. Pakrashi, Vibration energy harvesting based monitoring of an operational bridge undergoing forced vibration and train passage, Mechanical Systems and Signal Processing 106 (2018) 265–283.

[28] P. Fitzgerald, A. Malekjafarian, B. Bhowmik, L. Prendergast, P. Cahill, C.-W. Kim, B. Hazra, V. Pakrashi, E. Obrien, Scour damage detection and structural health monitoring of a laboratory-scaled bridge using a vibration energy harvesting device, Sensors (Switzerland) 19 (11).

[29] Y. Song, Finite-element implementation of piezoelectric energy harvesting system from vibrations of railway bridge, Journal of Energy Engineering 145 (2) (2019) 04018076

[30] K. Takeya, E. Sasaki, Y. Kobayashi, Design and parametric study on energy harvesting from bridge vibration using tuned dual-mass damper systems, Journal of Sound and Vibration 361 (2016) 50–65

[31] S. Priya, D. J. Inman, Energy Harvesting Technologies, 1st Edition, Springer Publishing Company, Incorporated, 2008.

[32] N.G. Stephen, On energy harvesting from ambient vibration, Journal of Sound and Vibration 293 (1) (2006) 409 – 425.

[33] S. Roundy, P.K. Wright, J. Rabaey, A study of low level vibrations as a power source for wireless sensor nodes, Computer Communications 26 (11) (2003) 1131–1144

[34] N.E. DuToit, B.L. Wardle, S.-G. Kim, Design considerations for mems-scale piezoelectric mechanical vibration energy harvesters, Integrated Ferroelectrics 71 (2005) 121–160

[35] C.B. Williams, R.B. Yates, Analysis of a micro-electric generator for microsystems, Sensors and Actuators A: Physical 52 (1) (1996) 8 – 11

[36] G.-Q. Wang, Y.-M. Lu, An improved lumped parameter model for a piezoelectric energy harvester in transverse vibration, Shock and Vibration (2014) 935298

[37] A. Erturk, D.J. Inman, An experimentally validated bimorph cantilever model for piezoelectric energy harvesting from base excitations, Smart Materials and Structures 18 (2) (2009) 025009

[38] J. Li, H. Zhang, Moving load spectrum for analyzing the extreme response of bridge free vibration, Shock and Vibration (2020) 9431620

[39] CEN, EN 1991-2, Eurocode 1: Actions on Structures - Part 2: Traffic loads on bridges, European Committee for Standardization, Brussels, 2002.

[40] A. Doménech, M.D. Martínez-Rodrigo, A. Romero, P. Galvín, On the basic phenomenon of soil-structure interaction on the free vibration response of beams: Application to railway bridges, Engineering Structures 125 (2016) 254 – 265.

[41] P. Museros, E. Moliner, M.D. Martínez-Rodrigo, Free vibrations of simply-supported beam bridges under moving loads: Maximum resonance, cancellation and resonant vertical acceleration, Journal of Sound and Vibration 332 (2012) 326–345.

[42] Deutsches Institut für Normung, DIN 45672 Teil 2: Schwingungsmessungen in der Umgebung von Schienenverkehrswegen: Auswerteverfahren (1995).

[43] P. Galvín, A. Romero, E. Moliner, G. De Roeck, M.D. Martínez-Rodrigo, On the dynamic characterisation of railway bridges through experimental testing, Engineering Structures (2020) 111261

[44] E. Reynders, System identification methods for (operational) modal analysis: Review and comparison, Archives of Computational Methods in Engineering 19 (1) (2012) 51–124.